Dramatical hydro-sedimentary changes induced by bamboo fences over mangrove tidal flat of the largest delta in Beibu Gulf, southwestern China

Zuming Huang[1, 2], Zhijun Dai[1, 2*], Riming Wang[3], Xiaoyan Zhou[2], Wenhong Pang[2], Jiejun Luo[2], Bingbin Feng[4], Baoqing Hu[4*]

[1] Guangxi Key Laboratory of Marine Environmental Change and Disaster in Beibu Gulf, Qinzhou 535011, China

[2] State Key Laboratory of Estuarine and Coastal Research, East China Normal University, Shanghai 200062, China

[3] Key Laboratory of Coastal Science and Engineering/Qinzhou Key Laboratory for Eco-Restoration of Environment, Beibu Gulf University, Guangxi 535011, China

[4] Key Laboratory of Environment Change and Resources Use in Beibu Gulf (Nanning Normal University), Ministry of Education, Nanning 530001, China

Abstract

Mangrove forest is one of the most important ecological and environmental resources by effectively promoting tidal flat deposition and preventing the coastal region from typhoon. However, there have been mass loss of mangrove forests due to anthropogenic activities. It is an urgent need to explore an effective way for mangrove restoration. Here, three rows of bamboo fences with hydro-sedimentary observation set over *Aegiceras corniculatum* mangrove tidal flat of the Nanliu Delta, the largest delta of Beibu Gulf, China, were conducted to analyze the hydro-sedimentary variations induced by bamboo fences. Results identified that the mean horizontal velocity U_m per burst (20 min) decreased by as much as 71% and 40% in comparison with those without bamboo fences in March and November, respectively, when the tidal current entering the bamboo area during flood. The maximum of mean horizontal flow velocity U_{m-max} at bamboo area was 50%–75% of that without bamboo fences during ebb tide. The suspended sediment concentration of bamboo area suggested a maximum reduction of 57% relative to bare flat during flood, and was 80% lower than bare flat at ebb peak. Moreover, the turbulent kinetic dissipation ε at flood tide was significantly higher than that at ebb tide, while the bamboo fences greatly increased the turbulent kinetic dissipation ε by 2 to 5 times relative to bare flat, resulting in an increase of the bed elevation by inhibiting the sediment incipient motion and intercepting suspended sediment. The siltation rate at the bamboo area was 140% and 29.3% higher than that at the bare flat and the region covered with *A. corniculatum*, respectively. These results highlight that bamboo fences can effectively attenuate tidal current and thus promote siltation over mangrove flat, which contribute great benefit to mangrove survival.

Key words: mangrove tidal flat, bamboo fences, hydro-sedimentary process, bed siltation

1 Introduction

Mangrove forest generally grows in the intertidal zone of tropics or subtropics where land and sea interact frequently, which is a natural barrier against floods and storm surges (Murray et al.,2019; Van Der Stocken et al., 2019; Dai et al., 2021). However, one-third of the mangroves on earth have been permanently lost in the past 30 to 60 years, due to human activities such as intensive reclamation, land reclamation and coastal construction (Atwood et al., 2017; FAO, 2020; Dai et al., 2021). Furtherly, in the context of global warming, natural sedimentation rate of mangrove forests may not be able to catch up with rapidly sea level rising (SLR), which could produce extremely difficulty in the restoration of global mangrove forests (Murray et al., 2022). At the same time, the increased frequency and duration of coastal submergence due to SLR will also threaten the survival and growth of mangrove seedlings (Analuddin et al., 2020), eventually leading to tidal flat erosion (Woodroffe, 1995). For instance, nearly 69% of surface elevations increasing in the Indo-Pacific coastal region are slower than the local SLRs, where mangroves could be completely submerged as early as 2070 under sediment supply deficiency (Lovelock et al., 2015). Therefore, it is of great urgency to explore an effective way to accelerate the siltation of mangrove flats so as to cope with rapid SLR.

Through field observations and laboratory models, it has been indicated that tidal flat vegetation including mangroves, can slow down current, attenuate wave height, and promote sediment settlement to silt up the flat surface (Paul et al., 2012; Hu et al., 2014, 2021, 2022; Montgomery et al., 2019). Early studies in

Vietnam and Australia suggested that mangrove forest can reduce wind wave and swell heights by up to 20% every 100 m and increase the surface elevation at a rate of 0.1 cm/a (Mazda et al., 1997; Furukawa et al., 1997; Brinkman, 2006). Maza et al. (2017) found that the flow velocity and turbulent kinetic energy decreased by 50% and increased by 5 times in the root of mangrove edge region, respectively, which correspondingly caused the drop of suspended sediment in water and enhanced the flat elevation. Besides, tidal flat itself also has a certain influence on hydrodynamic dissipation and suspended sediment deposition due to topographic slope and sediment differences (Gong et al., 2017). Specifically, van Santen et al. (2007) conducted hydrological observations on the mangrove tidal flats of Vietnam estuary and showed that sediment incipient motion and deposition mainly occurred in the bare flat with strong waves and currents. Through experiments with large-scale hydrodynamic simulation devices, Stefanon et al. (2010) revealed that the bed slope of tidal flat may increase the intensity of water flow around the corner during spring and ebb tide, which further erode shoreline and coarsen sediment. Gong et al. (2017) showed that slope change of tidal flat prone to a large head difference through laboratory physical model, which intensified the scouring of tidal flat and reduced the flat elevation ultimately. Similarly, recent study found that when the terrain becomes steeper, the elevation of mangrove forests gradually decreases compared with SLR, and the siltation rate of flat is more likely to be affected by the decrease of vegetation density, thus mangrove forests gradually lose the ability to capture sediment (Horstman et al., 2015). Furtherly, wetland expansion and deposition are limited in the natural state, so scientists and relevant governments are trying to expand land resources through tidal flats siltation promotion by using indoor and outdoor experiments via artificial materials.

Since the 11th century, coastal countries, like China, the Netherlands, the United States, have relied on impermeable hard structures such as groins, offshore and submerged breakwaters to intercept the fluvial sediment, and carry out reclamation to elevate the beach surface (Bulleri and Chapman, 2010; Morris et al., 2018). However, these structures are subjected to hydrodynamic impacts all year round, combined with the leakage of themselves, foundation settlement, and flat erosion, which can easily cause local land damage and destroy the ecological environment along natural coasts (Li et al., 2007; Santa Barbara-University of California, 2017). Thereafter, in recent years, green structures based on ecological silting promotion have gained global attentions, especially the bamboo fences. For instance, Dutch kwelders have used wooden fences for ages to stimulate sedimentation in mangroves tidal flat and indicated that wave damping increases as wooden fence thickness and density of woody material increases in the Mekong Delta (Dao et al., 2018). Additionally, Dao et al. (2020) investigated the resistance of a wooden fence by determining the hydraulic gradient under stationary flow and discovered that the drag coefficient depended on the fence's porosity and Reynolds number strongly. Mai Van et al. (2021) compared the wave strengths in front of and behind the bamboo fences simultaneously, finding that the sedimentation occurred rapidly in the shelter areas by weakening wave. However, most of the researches above focus on wave attenuation in bamboo fences, how the tidal current is affected through field observations is still unclear, especially the mangrove tidal flats in the northern Beibu Gulf of China.

As the largest delta in the Beibu Gulf, China (Fig.1a), Nanliu Delta feeds approximately 45% of the gulf's mangrove forests. However, the delta has experienced a sharp decline in sediment discharge and an obvious change in mangroves area in the past half century (Long et al., 2022). Converted aquacultural ponds and the behavior of sea ducks along banks are the main reasons for the huge losses of mangrove forests and the siltation rate of tidal flats is likely to be lower than SLRs without effective intervention (Long et al, 2022). Although the local government tried to replant mangroves for ecological restoration, the presence of sea wall makes it impossible to accelerate the sedimentation of tidal flats seaward to provide a living environment for mangroves instead thus is the only way. Therefore, the possibility of bamboo fences was investigated in this study with the aim to clarify the role of bamboo fences in hydrodynamic and sedimentation of mangrove tidal flats. Main objectives include: (1) examine the effects of bamboo fences on near-bed flow velocity; (2) reveal the near-bed suspended sediment concentration (SSC) variations of mangrove tidal flat with or without settling of bamboo fences. The results derived from this study can provide a scientific basis for mangrove restoration and ecological engineering construction to resist coastal disasters.

2 Data and methods

2.1 *Field sites setting and zonation*

Located in the north of Lianzhou Bay (Fig. 1b), Qixing Island is an important mangroves growth region of Nanliu Delta with widely distributed shoals and sandbars, which serves as the study area of this work. Qixing Island is dominated by irregular diurnal tides with an average tidal range of 2.46 m and a maximum tidal range of 5.36 m (Zhou et al., 2022). The mean values of the flood and ebb tidal currents in the spring tide are respectively 0.62 m/s and 0.58 m/s. The average wave height is 0.3 m approximately. The population of *Aegiceras corniculatum* is the dominating native species of mangroves in Qixing Island where the vegetations are generally low with ages of 1–6 years seaward (Long et al, 2022).

Bamboo strips insertion was conducted at bare flat in the middle tidal flat of Qixing Island in January 2021. The bamboo fences consisted of three rows of strips running parallel to the seawall from northeast to southwest. The first row of bamboo fences is 33 m wide near the sea. The second and third rows are 32 m and 32 m wide respectively, with a spacing of 10 m between rows (Fig. 1c). Besides, bamboo strips (30 cm high, 3 cm wide and 3 mm thick) were inserted 20 cm into the mud for fixing, exposed only 10 cm to the ground (Fig. 1d).

2.2 *Instrument set up*

Mangroves tidal flat is not conducive to walking, and the thunderstorms in summer on Qixing Island furtherly increase the difficulty of observation. Therefore, two hydrodynamic observations were carried out at *A. corniculatum* tidal flat of Qixing Island in spring and autumn, while the effect of sedimentation over half a year could be also observed.

The first observation was arranged from 8 to 12 March in 2021 with two transverse transects that covered four consecutive 4 tidal cycles during spring tide. Transect A was composed with 4 measurement stations A1–A4 across the bamboo fences, of which A4 was in the bare flat, A3 was in the middle of the second and third row of bamboo fences, while A2 and A1 were respectively located at the edge and interior of *A. corniculatum*. Among them, A4 and A2 were equipped with Acoustic Doppler Velocimeter (ADV, 6-MHz vector current meter, Nortek AS, Rud, Norway) to record high-resolution 3-D flow velocity (u, v and w), flow direction (D_c) and water depth (h). Three probes of ADV were placed
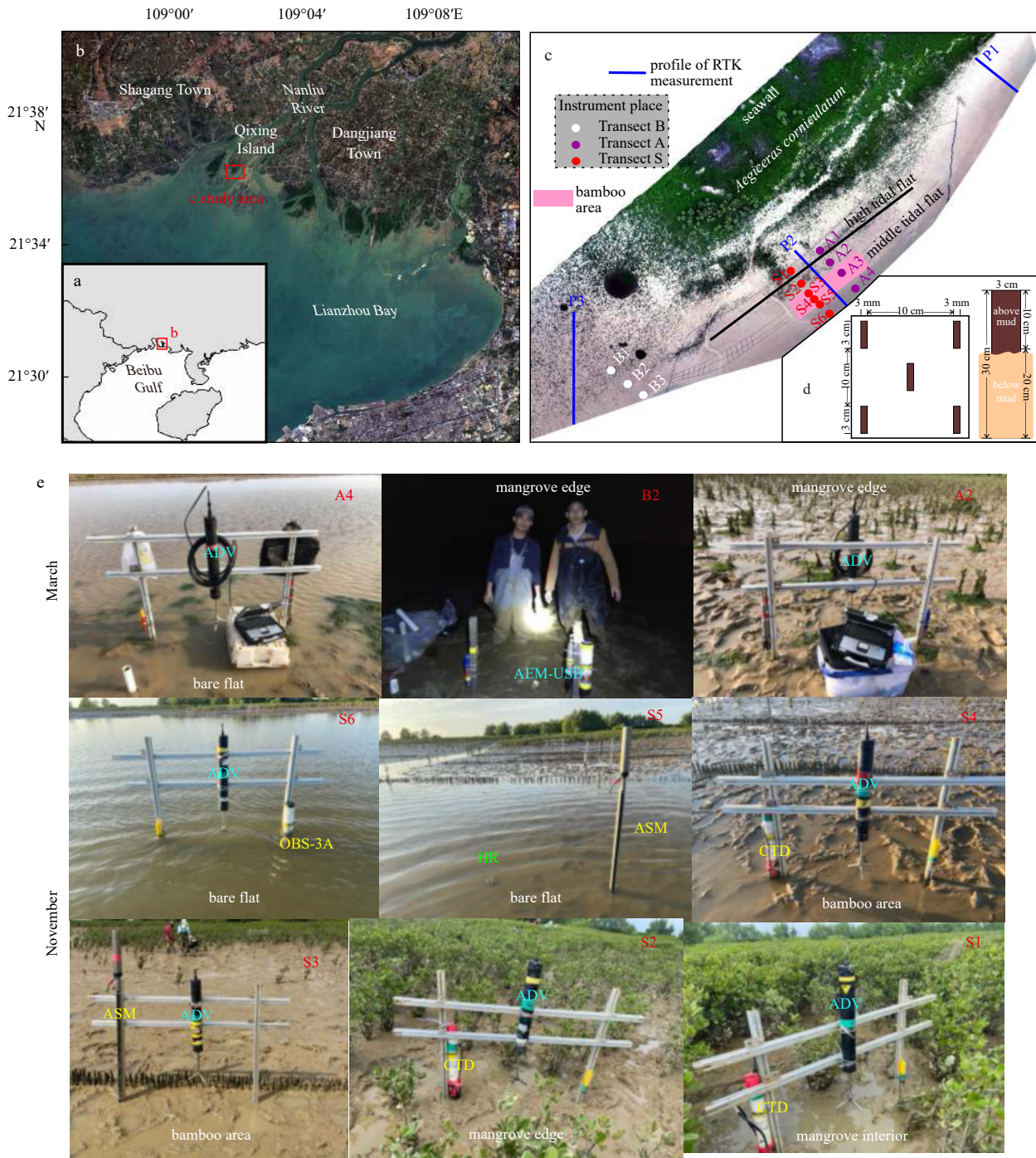
Fig. 1. Study area and instrument deployment. a. The location of Beibu Gulf; b. the location of Nanliu Delta and Qixing Island; c. the study area of Qixing Island with the bamboo fences, hydro-sedimentary instruments and GPS-RTK profile deployment; d. the parameters of bamboo strip; e. field pictures of instrument deployment in March and November. ADV: Acoustic Doppler Velocimeter; OBS-3A: Optical Backscattering Sensor; ASM: Argus Surface Meter; CTD: conductivity, temperture, depth; HR: high resolution.

down, 30 cm away from the bed surface, recording 4 800 measurements at a frequency of 8 Hz every 20 min (Table 1). Meanwhile, A3 and A1 were equipped with AEM-USB (ALEC, at a measuring range of 0–±500 cm/s, an accuracy of ±1 cm/s) buried in the ground with the probe exposed 10 cm to record 15 mean flow velocity and direction data per 20 min. Transect B was laid in the normal area without bamboo fences, where three measuring points B3, B2 and B1 were located at bare flat, the edge and interior of *A. corniculatum* respectively. Each station of Transect B were equipped with AEM-USB to measure near-bed flow data

above (Table 1).

The second observation was laid at Transect S with 6 measurement stations S1–S6 next to the Transect A of first observation across the bamboo fences during 6–10 November in 2021, recording both hydrodynamic and SSC. S6 and S5 were located at bare flat, of which S5 was deployed in the edge of the first row of bamboo fences. Stations S4 and S3 were set in the middle of the first and second rows, and close to the third row of bamboo fences (still within the bamboo area), whereas S2 was in the annual low *A. corniculatum* edge, and S1 was located between bien-

Table 1. Instrument setup and related obtained parameters during the observation

Instrument	Related obtained parameter	Sample rate/Burst (interval)	Measurement location above seabed/cm	Instrument site	Time
ADV	turbulent velocity, flow direction, water depth	8 Hz/20 min	15	A2, A4	8–12, March
ALEC	flow velocity, flow direction, water depth	15 samples/20 min	10	A1, A3, B1, B2, B3	
ADV	turbulent velocity, flow direction, water depth	32 Hz/20 min	15	S1, S2, S3, S4, S6	
HR-Profile	flow velocity, flow direction, water depth	4 Hz/20 min	0	S5	7–10, November
OBS-3A	turbidity	10 Hz/1 min	10	S6	
ASM-IV	turbidity	4 Hz/20 min	−10	S3, S5	
RBR-CTD	turbidity	0.1 Hz/consecutive	10	S1, S2, S4	

nial medium and low *A. corniculatum* in the high tidal flat. The instruments at each station of Transect S were equipped as follows: (1) All stations, except S5, were equipped with ADV, recording 19 200 measurements at a frequency of 32 Hz every 20 min (Table 1). (2) Flow velocity and water depth data were collected for the S5 through HR-Profiler (Nortek AS, Rud, Norway) which was buried underground with the probe up, while its blind area and sampling height were 40 cm and 50 cm respectively, and its sampling frequency was 4 Hz. (3) Near-bed turbidity at all sites were measured by Optical Backscattering Sensor (OBS-3A, D&A Instrument Company, Port Townsend, Washington, DC, USA), or Argus Surface Meter ASM-IV (Argus Company, Ritterhude, German) or CTD (RBRconcerto, RBR Company, Ottawa, Canada). The setting frequency and instruments placement height are shown in Table 1.

In addition, GPS-RTK at an accuracy of ±2 cm was used to measure elevation of tidal flat twice on January 30 and November 10. Three profiles were selected throughout entire bamboo fences, specifically, P1 (45 m long) and P3 (80 m long) were in the normal area without bamboo fences, P2 (55 m long) across bare flat—bamboo area—mangrove interior landward. All elevations of measured profiles were calibrated to the local mean sea level.

2.3 *Data processing*

2.3.1 *Data quality control of ADV*

As high-frequency data are extremely susceptible to noise contamination, the recorded 3-D velocities of the ADV require quality control before turbulence characteristic parameters calculations. Every time series of 20 min was processed as follows: (1) clear the 3-D velocities of low Signal-Noise Ratio (<5 dB) and low correlation (<70%) (Chanson et al., 2008); (2) remove the noises from the time series of velocity fluctuations by Phase-space-thresholding method proposed by Goring and Nikora (2002); (3) fill in the blank values with last valid data points, instead of the fitting interpolation method that may cause greater numerical distortion (Parsheh et al., 2010).

2.3.2 *Calculation of turbulent kinetic energy*

Turbulent kinetic energy (TKE) has been widely used to detect the influence of turbulent flow motions on sediment suspension in the nearshore area (Christensen et al., 2018; Pang et al., 2020, 2021):

$$\text{TKE} = \frac{1}{2}\rho(u'^2 + v'^2 + w'^2),\qquad(1)$$

where u', v' and w' refer to the x, y and z components of turbulent oscillation, and ρ=1 025 kg/m³ is the density of seawater. Taking x direction as an example：

$$u(t) = \bar{u} + u_w(t) + u'(t).\qquad(2)$$

In the turbulent boundary layer, instantaneous flow velocity

$u(t)$ is decomposed into mean flow component $\bar{u}$, wave orbital motion component $u_w(t)$ and turbulence component $u'(t)$. In these observations, all stations were equipped with T-wave to collect the significant wave height. Although most of the wave height were less than 10 mm, cannot reach the accuracy requirement of 5 mm, wave components still exist in part of the burst when water depth was large (Figs 2b, e). Clearly, it would be necessary to filter the wave motion to obtain accurate turbulent parameters. Considering the high-frequency turbulence but low-frequency wave, Fast Fourier Transform and Inverse Fast Fourier Transform (FFT-IFFT) were used to conduct high-pass filtering for the original data collected by ADV. Firstly, time series of 3-D velocities processed through Section 2.3.1 were transform into spectrum via Eq. (3).

$$X(k) = \sum_{j=1}^{N} x(j)\, e^{\frac{(-2\pi i)(j-1)(k-1)}{N}},\qquad(3)$$

where k represents the number of samples of the signal in the frequency domain, and N is the number of sampling, 9 600 in March and 19 200 in November. The selection of cut-off frequency for different bursts during de-wave was calculated from Eq. (4) according to the water depth h (Wiberg and Sherwood, 2008). The deeper the water depth, the stronger attenuation of high-frequency signal by water layers.

$$f_{\text{tidal cycle,max}} = \frac{1}{2}\sqrt{\frac{g}{\pi h}},\qquad(4)$$

where, h is the water depth. Then the low-frequency 3-D velocities below $f_{\text{tidal cycle,max}}$ in the frequency domain were set to zero, and finally the filtered frequency domain data was converted into the time domain via Eq. (5), while the real parts were taken as filtered flow velocities.

$$x(j) = \frac{1}{N}\sum_{k=1}^{N} X(k)\, e^{\frac{-(-2\pi i)(j-1)(k-1)}{N}}.\qquad(5)$$

2.3.3 *Estimation of turbulent energy dissipation*

Turbulent kinetic energy dissipation ε is determined according to the "−5/3" power law in the inertial subrange based on Kolmogorov's theoretical spectrum (Liu and Wei, 2007):

$$S_i(k) = \alpha_i \varepsilon^{\frac{2}{3}} k^{-\frac{5}{3}},\qquad(6)$$

where k is wave number, $S_i(k)$ represents the power spectral density of i velocity component ($i= x, y, z$). Under the local isotropic turbulence conditions, α_i is the one-dimensional Komolgorov universal constant which has been experimentally determined, α_x=0.51, α_y=α_z=4/3α_x=0.68 (Green, 1992). Since velocity ob-
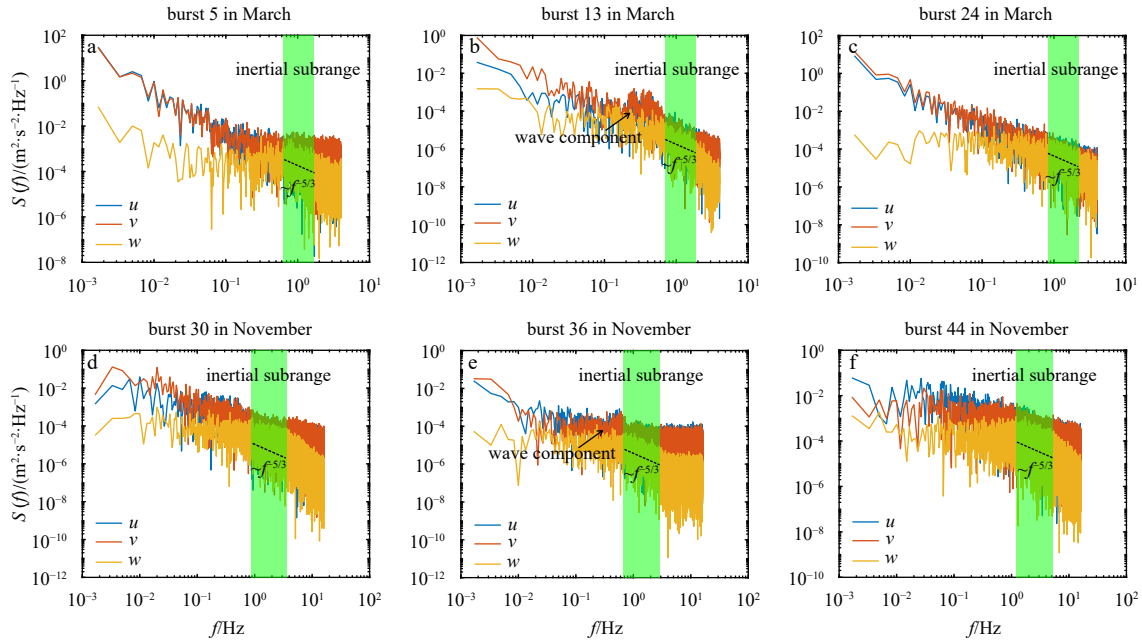
Fig. 2. Energy spectrum of velocity fluctuations (*u*, *v*, *w*) observed by Acoustic Doppler Velocimeter. a and d at the flood peak period in March and November; b and e at the slack water period in March and November; c and f at the ebb peak period in March and November.

servations by ADV follow a time series change at a point in space, the spectrum form of wave number *k* should be transformed into frequency spectrum (Huntley, 1988). Taylor (1938)'s "frozen turbulence" hypothesis is applied here,

$$k = \frac{2\pi f}{\overline{U}}, \tag{7}$$

$$kS_i(k) = fS_i(f), \tag{8}$$

where *f* is the sampling frequency, $\overline{U}$ refers to horizontal flow velocity. Combined with Eqs (6)–(8), the available frequency spectrum can be obtained as follow:

$$S_i(f) = \left(\frac{\overline{U}}{2\pi}\right)^{\frac{2}{3}} \alpha_i \varepsilon^{\frac{2}{3}} f^{-\frac{5}{3}}. \tag{9}$$

Vertical velocities are less contaminated by waves than horizontal velocities near bed (Liu and Wei, 2007). In this paper, stations A4 and S6 of bare flat were taken as examples to show the frequency spectrums of 3-D velocities during peak flood (Figs 2a, d), slack water (Figs 2b, e) and peak ebb (Figs 2c, f) in the first tidal cycle. As shown in Fig. 2, the vertical velocities *w* basically coincided with the slope of "−5/3" law in logarithmic coordinate, thus the fluctuations *w'* were selected to calculate the turbulent kinetic energy dissipation ε.

2.3.4 *Calibration of turbidimeter*

Resulting from sediment otherness induced different background values and accuracies of OBS-3A, ASM-IV and CTD at each station, there is no absolute quantitative relationship between SSC and turbidity (Butt and Russell, 1999; Pang et al., 2020). Thus, the relationship between turbidity and SSC of every turbidity meter was obtained through calibration in this paper. Firstly, the turbidity meters were fixed 10 cm away from the bot-

tom in the calibration bucket, then water was injected into the bucket and the spiral agitator was started before recording the initial turbidity. Thereafter, the mud collected next to turbidity meters in the field was dried and poured into the bucket slowly until the real-time values were stable for 1 min. The water sample of 550 cm³ near the probe was collected subsequently. Operations above were repeated until calibrated turbidity reached the maximum observation in the field. After filtering, rinsing, drying and weighing, the ratio of sediment weight to water sample volume was SSC, which was transformed through the fitting relationship as shown in Fig. 3. In particular, ASM-IV has 96 probes, and 10 of them were buried under mud during field observation, so the 75th to 85th probes were calibrated and averaged in this study.

Furthermore, mud samples near the measuring stations were taken for sediment grain size analysis by laser particle size analyzer *LS13 320*. The near-bed suspended sediment flux (SSF) was calculated according to the SSC and the mean horizontal velocity component perpendicular to bamboo fences,

$$\text{SSF} = \overline{U} \times \cos\theta \times \text{SSC}, \tag{10}$$

where θ refers to the angle between the horizontal flow velocity and bamboo fences.

3 Results

3.1 *Hydrodynamic variations*

3.1.1 *Hydrodynamic variations in the absence of bamboo fences*

During the spring tide from March 8 to 12 (4 tidal cycles marked as T1 to T4), the water depth *h* in the non-bamboo area increased seaward, with the maximum value occurring at T3 (Fig. 4a), when the h_{max} (the maximum of water depth) of B1, B2 and B3 stations were 2.04 m, 2.14 m and 2.31 m, respectively (Table 2). The mean horizontal flow velocity U_m of B1, B2 and B3
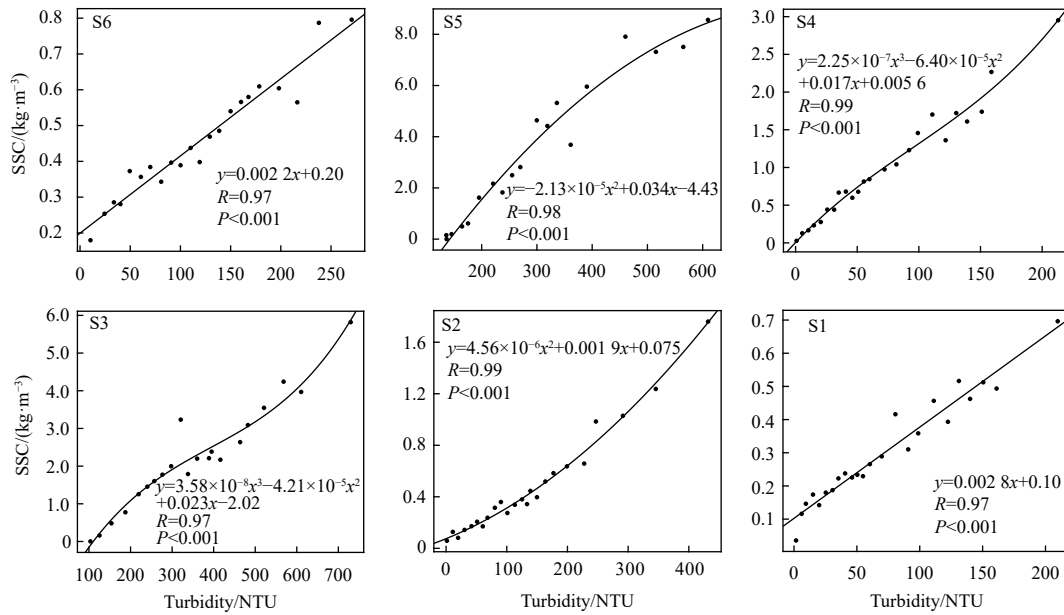
Fig. 3. Fitting curves between turbidity value and suspended sediment concentration (SSC) of the water samples for the stations with turbidity measurement. NTU is the unit of turbidity.

stations varied in the range of 0.03–0.28 m/s, 0.02–0.24 m/s and 0.01–0.18 m/s at flood tide, while the $U_{\text{m-max}}$ (the maximum of mean horizontal flow velocity) occurred in peak flood. The flow velocity U_{m} of B3 station was significantly greater than that of B1 and B2 during the ebb tide, with a maximum of 0.29 m/s, 61% and 53% higher than that of B1 and B2 (Table 2).

There was a significant deflection of flow at the edge of *A. corniculatum* forests (based on Nautical Coordinate). The flow spread from B3 to B2 along with the direction D_c varying from 330°–40° to 230°–90° during the flood tide (Table 2). Subsequently, the flow was counterclockwise deflected at the D_c between 292°–337°. During the ebb tide period, water flow always maintained a southeasterly directional motion at B1 station, followed by a clockwise deflection at B2 and B3, and the deflection amplitude gradually decreased from 150° to 24° as water depth h decreased (Fig. 4c). Furtherly, during the flood tide, the $U_{\text{pb-max}}$ (the maximum of mean horizontal velocity perpendicular to the bamboo fences) of B2 decreased by 22% compared with that of B3, while the $U_{\text{pb-max}}$ of B1 in *A. corniculatum* interior was the largest in Transect B, with an average of 0.18 m/s. However, the absolute $U_{\text{pb-max}}$ of B1 and B2 were both lower than that of B3, and the flow directions were mainly toward the shore (Table 2, Fig. 4d).

3.1.2 *Hydrodynamic variations in the area with bamboo fences*

In March 2021, the mean horizontal flow velocity U_{m} of the Transect A across the bamboo fences showed a symmetrical variation with the change of water depth h (Figs 4e, f). The $U_{\text{m-max}}$ indicated 0.55 m/s at A4 in bare flat, which was the largest velocity among all stations during flood tide, 29% higher than that of ebb tide (Table 2). With the flow entering into bamboo area, the flow velocity U_{m} at A3 decreased by 71% compared with A4 (0.18 m/s). However, the U_{m} at A2 at the edge of *A. corniculatum* forests increased again after across the bamboo fences, which made the curve of U_{m} in the middle of A4 and A3 (Fig. 4f). All the U_{m} at A1 in high tidal flat was less than 0.06 m/s. During the ebb tide, the velocities U_{m} spatially exhibited decreasing trend landward (Figs 4b, f). In addition, the flow direction D_c obviously diffused in A2

at the flood tide, with a range of 30°–75°, and the D_c of bare flat A4 was similar as that in *A. corniculatum* edge A2. The D_c of A1 varied between 100 and 300 subsequently. The ebb tide D_c of A1–A4 were basically in the southwest, and there was a clockwise and then counterclockwise deflection (less than 30°) at the edge of *A. corniculatum* and bamboo area. At the same time, the U_{pb} at A3 was obviously larger than that of other stations at both flood and ebb tide. A phenomenon of water reflection at A2 and A4 stations made the U_{pb} negative (Fig. 4g, Table 2).

In November 2021, the maximum water depth h at bare flat S6 varied between 1.8 m and 2.6 m during 4 tidal cycles (Fig. 4i). The mean horizontal flow velocity U_{m} at each station of Transect S obeyed the principle of symmetry like that in March, with the greatest values reaching 0.49 m/s at S6 and S5 during flood tide of T3 (Table 3). Different from March, the $U_{\text{m-max}}$ only decreased by 40%–50% after the flood water entered the bamboo area, and then increased to 0.31 m/s before leaving the bamboo area at S3 station (Table 3). Finally, when the flow transferred from bamboo area to *A. corniculatum*, the U_{m} dropped to less than 0.1 m/s (Fig. 4j). Meanwhile, the flood flow direction D_c from bare flat S5 to bamboo area S4 changed from northeast to southeast with an average of 53° clockwise during T1. The range of D_c was relatively concentrated compared with that in March. D_c of S2 at the edge of *A. corniculatum* forests was similar to A2, while the D_c at S1 inside the high tidal flat varied from 30°–90° (Fig. 4k). Moreover, the velocity perpendicular to the bamboo fences U_{pb} was the largest at bare flat, up to 0.08 m/s, whereas U_{pb} at S4 and S3 were negative and positive respectively which made the biggest difference of 0.065 m/s during T3 flood tide. Averaged U_{pb} of S1 and S2 were lower than 0.02 m/s like that of A1 and A2. During the ebb tide period, the U_{m} was the same as that in March, increasing seaward and the flow direction was first clockwise and then counterclockwise at *A. corniculatum* edge—bamboo area and bamboo area—bare flat. The value of the U_{pb} at S4 station was also small, lower than 0.01 m/s except for T3 (Fig. 4l).

3.2 *Suspended sediment transport at bamboo-inserted area*

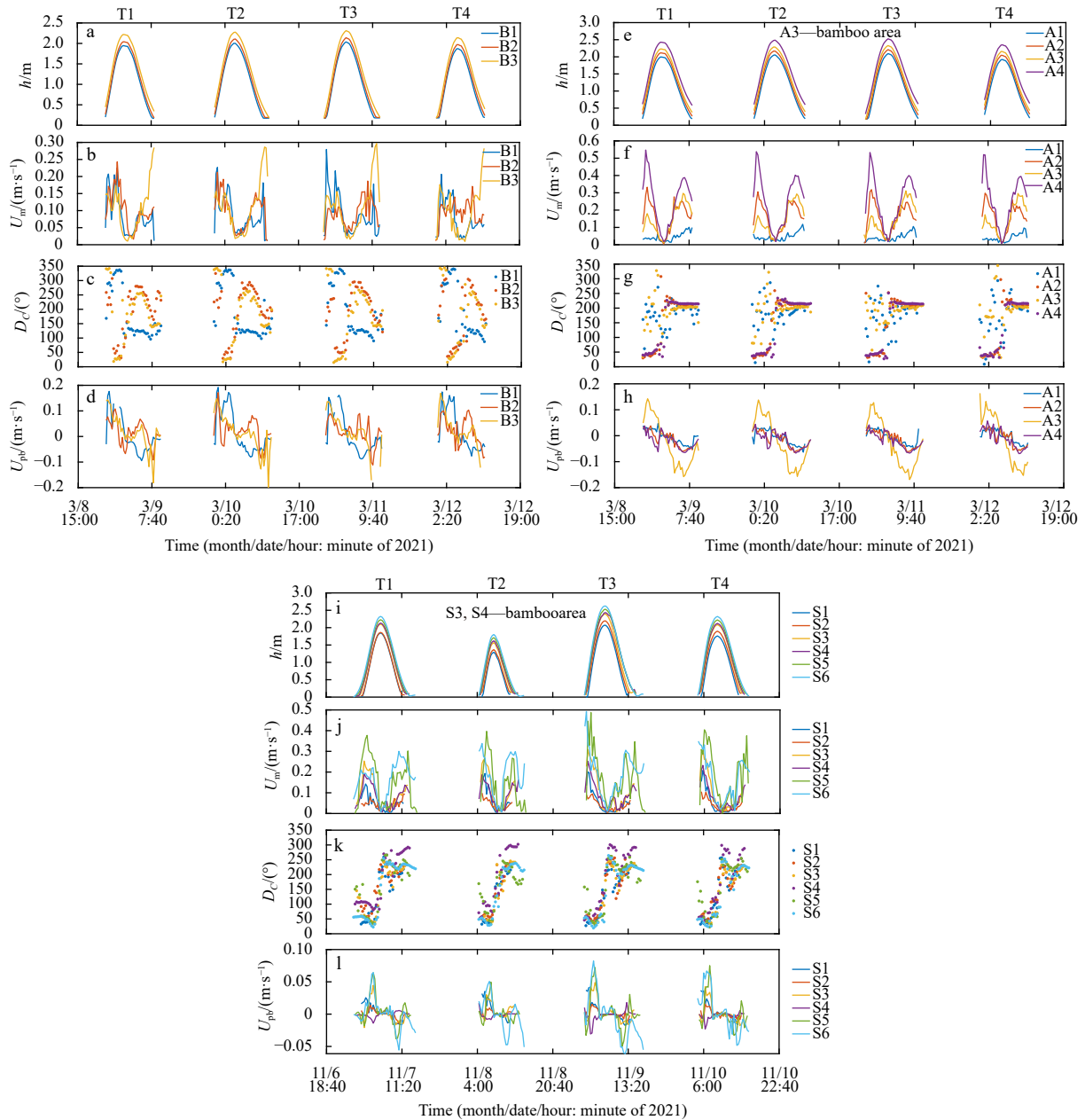SSC was obtained by substituting turbidity into the fitting for-

Fig. 4. Time series of a, e and i water depth *h*; b, f and j mean horizontal flow velocity U_{m}; c, g and k mean direction of the flow D_c; d, h and l mean horizontal velocity perpendicular to the bamboo fences U_{pb} at normal area and bamboo-inserted area in March and November, respectively. Stations A3, S3 and S4 were between the bamboo fences. T1–T4 refer to the first tide to the fourth tide in March and November.

mulas as shown in Fig. 3. During the observation period in November, the SSC of S3 and S5 during ebb tide were significantly higher than that during flood tide, while the rest stations suggested opposite tendency. During the flood tide, the SSC at S6 was low, ranging from 0.21–0.27 kg/m³. Compared with S6, the SSC at S5 in front of the first row of bamboo fences suddenly increased, and the maximum value was 3.5 kg/m³ during peak flood in T2. After entering the bamboo area, the SSC at S4 decreased with the maximum reduction rate equaling to 57% at T2 relative to S5, fluctuating in the range of 0.24–1.66 kg/m³. Subsequently, SSC between S3–S1 increased first and then decreased. The SSC at S3 in the bamboo area was always the largest from peak flood to peak ebb, but the value was less than 2 kg/m³ during this period. However, the SSC of S3 and S5 both increased

again from peak ebb to low tide, with a SSC$_{\mathrm{max}}$ of 5.59 kg/m³ and 8.63 kg/m³ (Fig. 5), while the SSC of S4 was 80% lower than that of S3 and S5.

As the SSF perpendicular to the bamboo fence, the sediment transported between S3–S5 mainly in the offshore, and the total transportation rate during the observation was 0.62 kg/(m²·s) (Table 4). However, the flow carried most of suspended sediment shoreward along S5–S6 with a flux of 0.46 kg/(m²·s), so that the sediment-carrying flux of onshore flow along S3–S6 were greater than 1.08 kg/(m²·s) at least. In addition, the SSF at S2–S3 were mainly shoreward, and the seaward transportation direction of SSF at S1–S2 between the high and middle tidal flats was the same as that of bamboo area. SSF at S1–S2 was smaller, accounting for 30.7% and 27% of S3–S4 and S2–S3, respectively (Table 4).

Table 2. Hydrodynamic characteristic values for 4 tidal cycles in March

Site	Tide	$U_{\text{m-max}}$/(m·s^{-1})	$h_{\max}$/m	Range of D_c/(°)	$U_{\text{pb-max}}$/(m·s^{-1})
A1	flood	0.04, 0.06, 0.04, 0.04	2.00, 2.06, 2.09, 1.92	100–300	0.05, 0.04, 0.03, 0.03
	ebb	0.10, 0.12, 0.11, 0.10		180–230	−0.05, −0.06, −0.06, −0.05
A2	flood	0.33, 0.31, 0.32, 0.30	2.12, 2.17, 2.21, 2.04	30–75	0.04, 0.04, 0.04, 0.04
	ebb	0.28, 0.25, 0.25, 0.26		205–240	−0.06, −0.07, −0.06, −0.06
A3	flood	0.18, 0.17, 0.17, 0.17	2.23, 2.49, 2.53, 2.35	35–330	0.14, 0.14, 0.13, 0.16
	ebb	0.29, 0.29, 0.31, 0.30		170–210	−0.15, −0.16, −0.17, −0.15
A4	flood	0.55, 0.54, 0.53, 0.52	2.43, 2.49, 2.53, 2.35	40–80	0.04, 0.04, 0.04, 0.06
	ebb	0.39, 0.40, 0.40, 0.39		210–220	−0.07, −0.07, −0.07, −0.07
B1	flood	0.21, 0.23, 0.28, 0.21	1.95, 2.00, 2.04, 1.87	280–340	0.18, 0.19, 0.16, 0.17
	ebb	0.1, 0.18, 0.18, 0.08		110–130	−0.1, −0.08, −0.11, −0.08
B2	flood	0.24, 0.21, 0.11, 0.14	2.04, 2.11, 2.14, 1.97	230–90	0.11, 0.17, 0.09, 0.1
	ebb	0.13, 0.14, 0.19, 0.17		230–290	−0.1, −0.09, −0.11, −0.08
B3	flood	0.17, 0.16, 0.15, 0.18	2.22, 2.27, 2.31, 2.14	330–40	0.14, 0.15, 0.14, 0.17
	ebb	0.14, 0.29, 0.29, 0.28		210–260	−0.18, −0.13, −0.19, −0.14

Table 3. Hydrodynamic characteristic values for 4 tidal cycles in November

Site	Tide	$U_{\text{m-max}}$/(m·s^{-1})	h/m	Range of D_c/(°)	$U_{\text{pb-max}}$/(m·s^{-1})
S1	flood	0.14, 0.19, 0.20, 0.21	1.85, 1.29, 2.07, 1.76	30–90	0.025, 0.035, 0.04, 0.036
	ebb	0.06, 0.05, 0.06, 0.06		140–230	−0.016, −0.014, −0.018, −0.016
S2	flood	0.08, 0.10, 0.09, 0.11	1.86, 1.37, 2.19, 1.90	40–120	0.014, 0.009, 0.015, 0.016
	ebb	0.09, 0.05, 0.07, 0.06		150–250	−0.015, −0.003, −0.013, −0.008
S3	flood	0.25, 0.26, 0.31, 0.30	2.10, 1.57, 2.39, 2.09	30–70	0.045, 0.03, 0.049, 0.042
	ebb	0.14, 0.16, 0.14, 0.13		180–240	−0.016, 0.012, −0.016, −0.018
S4	flood	0.19, 0.19, 0.25, 0.23	2.13, 1.62, 2.43, 2.12	40–110	−0.014, −0.008, −0.031, −0.023
	ebb	0.14, 0.16, 0.14, 0.14		200–300	0.007, 0.003, 0.02, 0.005
S5	flood	0.38, 0.4, 0.49, 0.40	2.22, 1.71, 2.53, 2.22	30–80	0.064, 0.05, 0.07, 0.05
	ebb	0.3, 0.27, 0.35, 0.38		210–265	−0.038, −0.015, −0.05, −0.033
S6	flood	0.22, 0.34, 0.49, 0.35	2.32, 1.80, 2.62, 2.32	20–70	0.064, 0.05, 0.08, 0.067
	ebb	0.3, 0.3, 0.31, 0.26		215–250	−0.056, −0.05, −0.061, −0.047
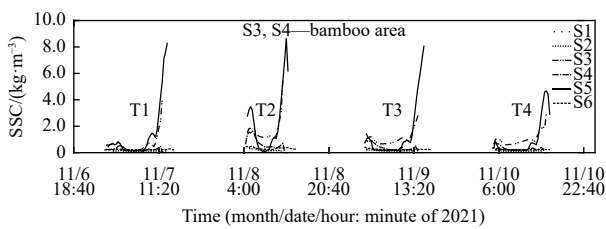
Fig. 5. Time series of suspended sediment concentration (SSC) at bamboo area in November. Stations S3 and S4 are between the bamboo fences.

3.3 *Changes in tidal flat elevation*

3.3.1 *Elevation variations in the absence of bamboo fences*

From January 30, 2021 to November 10, 2021, siltation occurred in profiles P1 and P3 in the normal area without bamboo fence, but there were significant differences in the siltation mor-

phology and thickness (Fig. 6). Located in the bare flat in front of *A. corniculatum*, Profile P1 was in the northeast of bamboo fences, and its elevation varied from 0.05 m to 0.55 m. In the past 9 months, the siltation thickness of profile P1 were uniform with an average of 49 mm. Meanwhile, the profile envelopes of P1 measured twice between 130 m and 160 m from the seawall were parallel, and the degree of inclination was flatter when it was closer to the sea (Fig. 6a). Profile P3 in the non-bamboo area was located directly west of the bamboo fences, with an elevation range of 0.39–0.58 m during the measurement period. The *A. corniculatum* interior—edge 115–155 m away from seawall of P3 was only silted up by an average of 28 mm in November relative to January. There were small erosion and large siltation at 10 m and 15 m from the edge, respectively, forming ripples and berms. In addition, the average siltation thickness of the bare flat 165–190 m from seawall was 38 mm, where the latter 20 m of P3, similar to the morphology of P1, was relatively flat with the two envelopes nearly parallel (Fig. 6c).

Table 4. Variation of suspended sediment flux at bamboo-inserted area in November (unit: kg/(m²·s))

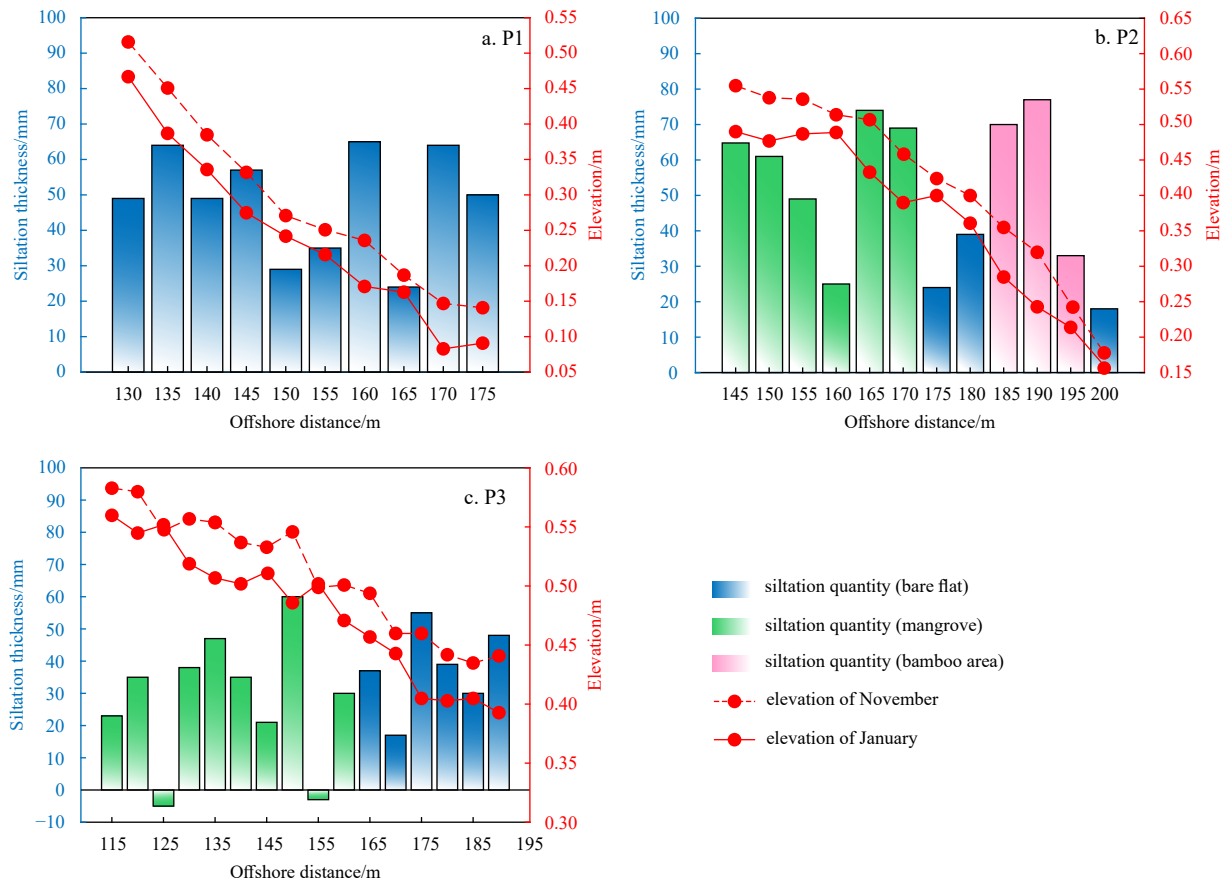|	T1		T2		T3		T4		Total
	flood	ebb	flood	ebb	flood	ebb	flood	ebb	net difference
S6	0.055	−0.061	0.10	−0.074	0.11	−0.15	0.11	−0.076	0.46
S5	0.027	−0.035	0.004 4	−0.23	0.000 89	−0.086	0.028	−0.15	−0.29
S4	−0.019	0.010	−0.038	−0.001 9	−0.072	0.005 8	−0.032	−0.003 9	−0.33
S3	0.028	−0.13	0.14	0.11	0.17	−0.13	0.082	−0.092	0.17
S2	0.005 9	−0.007 9	0.007 6	0.000 54	0.008 5	−0.004 3	0.005 2	−0.005 6	−0.089
S1	0.027	−0.016	0.059	−0.008 9	0.047	−0.016	0.037	−0.014	

Fig. 6. Changes of elevation and siltation thickness of tidal flat profiles P1 and P3 at normal area, P2 at bamboo-inserted area offshore distance for 9 months.

3.3.2 *Elevation variations in the area with bamboo fences*

Profile P2 was 55 m in length from *A. corniculatum* interior to sea across the bamboo area, and its elevation varied from 0.15 m to 0.56 m. Compared with P1 and P3, P2 presented the most obvious siltation effect (Fig. 6b). The most obvious siltation occurred at the *A. corniculatum* edge and bamboo area which were 165–180 m and 185–190 m offshore respectively, both with the elevation increasing by more than 75 mm, and the berm that existed in January was submerged due to the siltation. The average siltation thickness of the 15–25 m section inside the *A. corniculatum* forests was 58 mm during the past 9 months. At the junction of high and middle tidal flats and 20 m from bamboo fences to the sea, the average sediment thickness was only 41.6% of bamboo area. Moreover, the spatial change of P2 profile was not gradual flattened or alternating like P1 and P3, but its absolute slope value increased uniformly. As a result, the area between bare flat and bamboo fences inclined increasingly with a slope of −0.014, where the envelopes no longer showed parallel siltation (Fig. 6b).

4 Discussion

4.1 *Hydrodynamic impacts of bamboo fences*

Waves and currents are the main dynamics in shaping coastal geomorphology, while the progressive process of tidal flat is influenced by bed roughness, vegetation, tidal level and so on (Horstman et al., 2014; Foster-Martinez et al., 2018). In addition to vegetation slowing down hydrodynamic by increasing bed surface roughness, waves and currents on bare flat also cause par-

tial energy loss due to substrate difference and terrain slope (Möller et al., 1999; Horstman et al., 2014).

Since the maximum distance between the measuring stations was 20 m, there was no significant difference in the mean median size D_{50}=0.091 mm at S1–S5. However, the submerged duration of S6 was longer than that of other stations, which created strong hydrodynamic for sediment coarsening, with a D_{50} of 0.11 mm. According to the classification methods of Shepard (1954) and Wentworth (1922), all the sediment at S1–S6 belonged to very fine sand, so the dynamical sedimentation process caused by different substrate sediment in this paper was considered to be the same. In addition, the topographic profile was divided into three segments, with the absolute slope values of S1–S2, S2–S4, and S4–S6 being 1.2‰, 8.2‰, and 9.1‰, respectively (Fig. 7). Note that S1–S2 was mainly located in the high tidal flat with *A. corniculatum*, where the tidal current dissipation was mainly affected by vegetation and therefore will not be considered in the discussion below.

As the velocity U_{pb} attenuation per unit distance, r was calculated respectively taken S6 and S2 as incident stations during flood and ebb tide. The fluctuation of r value at flood tide was significantly greater than that at ebb tide, especially at station S4 being located in the first and second row of bamboo fences (Fig. 8). In the case of the same substrate sediment and distance intervals, the smaller the velocity U_{pb} difference between any two stations was, the smaller the r value was, indicating that the influence of topographic slope was greater than vegetation or bamboo fences during flood tide, and the opposite was true at ebb tide. For instance, S5 and S6 were all located in the bare flat, with the r value
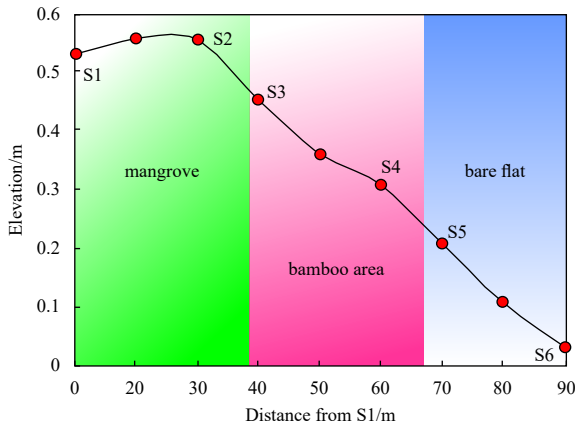
Fig. 7. Topographic slope change along the profile in November.

at S5 being the minimum among S1–S5 during flood tide, manifesting that there was little difference in tidal current actions between the two stations (Fig. 8), except for relatively large *r* value in the early flood tide when the instrument HR working improperly due to shallow water depth. However, flow reflection made a big difference in the flow velocity U_{pb} at S4 due to the direct blocking effect of bamboo fences, and the maximum *r* value at 5:00 at T1 was 125 times of that at S5. Subsequently, *r* value

between the second and third bamboo fences at S3 was closed to the edge of *A. corniculatum* at S2, varying between −0.000 2 (m/s)/m and 0.001 75 (m/s)/m. Between high tide and peak ebb, the upper flow was not directly blocked by obstacles and the inertia made the water column easily pass through after the tide water inundated the mangroves and bamboo fences, which contributed to the small *r* value relatively at each station. There was no obstacle between S5 and S6 stations so that the *r* value of S6 was larger than other stations from peak ebb to low tide, especially reaching 0.000 8 (m/s)/m at T2. The increase of *r* value during ebb tide indicated that the potential energy generated by the slope of tidal flat led to the increase of flow velocity, which reflected the barrier effect of bamboo fences and *A. corniculatum* forests.

Taken altogether, bamboo fences induced currents slowing was considerably stronger than tidal flat topographic slope and substrate sediment differences. Bamboo area served as the edge of *A. corniculatum*, resulting in the largest hydrodynamic dissipation during flood tide, whereas played a role to extend *A. corniculatum* edge seaward during ebb tide.

4.2 *Impacts of bamboo fences on sediment deposition*

Bottom shear stress is an important indicator to evaluate the strength of hydrodynamic in tidal flat, and the current-induced bottom shear stress is a vital factor for identifying the distribu-
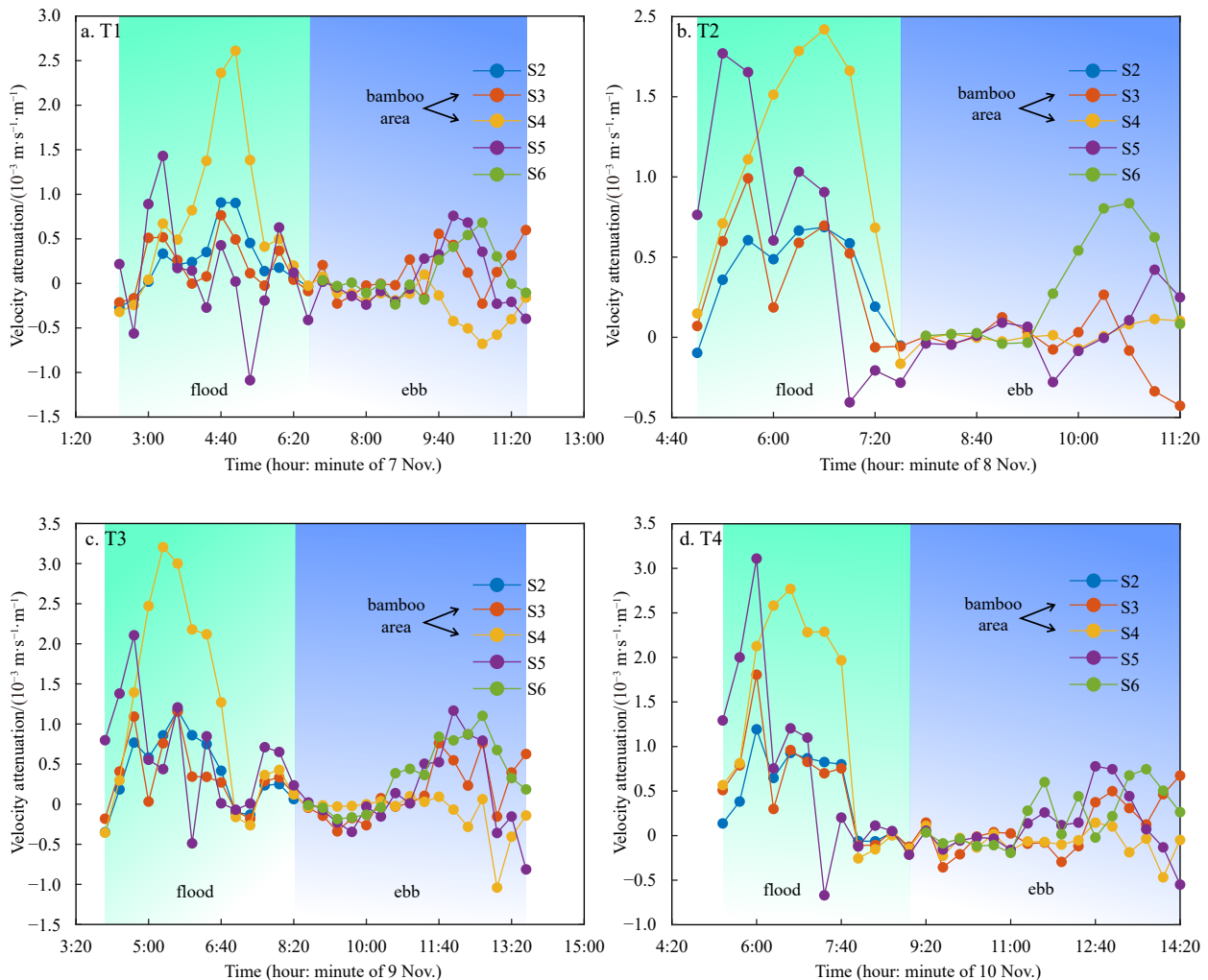

Fig. 8. Time series of velocity U_{pb} attenuation rate *r* during T1 (a), T2 (b), T3 (c), and T4 (d) in November.

tion of suspended sediment in meso-macro tidal flat (Zhu et al., 2017; Pang et al., 2020). The generation of near-bed turbulent energy is equal to dissipation, which makes the current-induced bottom shear stress is proportional to TKE (Stapleton and Huntley, 1995). By fitting the relationship between TKE of November and SSC through exponential function, it is showed that TKE was significantly correlated with SSC in bare flat, bamboo area and mangrove forests (Fig. 9). Thereafter, the turbulent kinetic energy dissipation ε calculated in Section 2.2.3 can be used to reveal the sediment interception mechanism of bamboo fences.

In March, the turbulent kinetic dissipation ε at bare flat (A4) was significantly higher than that of the *A. corniculatum* edge (A2) during flood tide (Fig. 10a). Subsequently, the ε during slack water and low tide turned much lower, with an average value of 2.08×10^{-5} m$^2\cdot$Hz/s^2 at A2 station and 1.49×10^{-5} m$^2\cdot$Hz/s^2 at A4 station. When the flood water passed through the bamboo fences from station A4, all the flow velocity U_m at A2 decreased by more than 40% (Fig. 4f), and the TKE reduced accordingly at bamboo area where it became the main deposition area of suspended sediment. In November, the change of ε fully proved above deduction. During flood tide period, the variation ranges of ε at S6 were basically the same as A4 in March, with the ε_{max} ranging between 0.2×10^{-3}–1.2×10^{-3} m$^2\cdot$Hz/s^2, which was also apparently higher than S2 at the edge of *A. corniculatum* (Fig. 10b). Meanwhile, the ε in bamboo area (S3 and S4) was 2 to 5 times of that in bare flat (S6), suggesting an maximum ε_{max} of 2.48×10^{-5} m$^2\cdot$Hz/s^2. However, the flow velocity U_m in bamboo area was 40% or less of that in the bare flat (Fig. 4j), highlighting the dissipative effect of bamboo fences on turbulence instead of large vertical velocities. The increased turbulent kinetic energy dissipation led to a sharp decrease in TKE in bamboo area, thus weakening the sediment
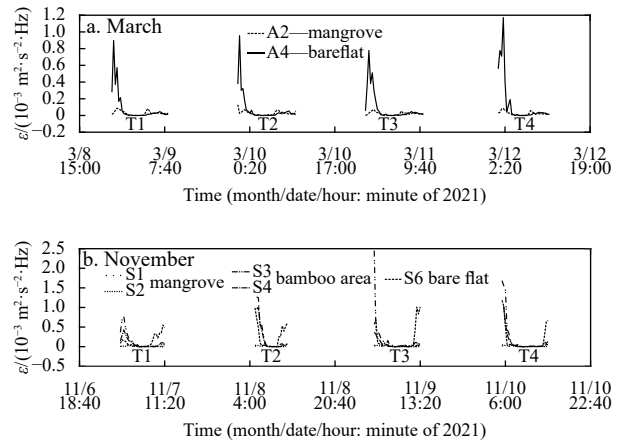

Fig. 9. Exponential fitting between suspended sediment concentration (SSC) and turbulent kinetic energy (TKE) in bare flat (a), bamboo area (b) and mangrove (c).

Fig. 10. Time series of turbulent dissipation rate ε at stations A2 and A4 in March (a) and stations S1, S2, S3, S4 and S6 in November (b).

incipient motion and decreasing the SSC, which was less than that at bare flat (Fig. 5). Compared with bamboo area, there was lower ε but higher TKE at bare flat where the sediment was easy to carry up. Then the suspended sediment deposited at S3 and S4 stations because of the direct blocking of bamboo fences and the indirect dissipation of sediment carrying by water flow, resulting in the rapid siltation and up-convex flat (Fig. 6b). During the ebb tide, the ε in bamboo area was close to or slightly greater than that in *A. corniculatum*, and then the sharp rise of ε in bare flat reduced the loss of SSF in the entire study area (Tables 3 and 4).

Generally, bamboo fences captured suspended sediment and inhibited sediment incipient motion by slowing down flow velocity and increasing turbulent kinetic energy dissipation respectively during flood tide, and served as *A. corniculatum* to delay the increase of turbulent intensity during ebb tide. The dynamical and sedimental differences of suspended sediment between the ebb and flood tide contributed to a stable siltation in bare flat, whereas rapid siltation occurred in bamboo area as in *A. corniculatum.* Above mechanism changed the profile from concave-up to convex-up (Fig. 6), and the associated morphological response shifted from scour to siltation (Friedrichs, 2011).

4.3 *Prospect of bamboo fences-based coastal restoration*

A combination of retaining existing seawalls and adopting innovative technologies is the most desirable approach to protect beaches and promote siltation (Foti et al., 2020). In this study, three rows of bamboo fences were deployed along the edge of mangrove forests under the premise of preserving the original seawall intactly. In terms of economy, the raw materials of bamboo strip come from the remolding of wood waste, which provided a strong guarantee for local materials. Meanwhile, the bamboo fences structure were simple to fabricate and their weight were so light that facilitates the carry and assemble in the field, eliminating a lot of heavy machinery and human resources costs for seawall heightening. In ecology respect, replaced concrete materials with the soft and degradable bamboo strip can avoid heavy metal pollution of seawater and tidal flat environment, which favored the survival of animals.

From the hydrodynamic perspective, the height of the bamboo strip used in this study was only 10 cm above the flat surface, which although may generate current circulation structure at the bottom during flood and ebb tide, the elastic contraction of wooden bamboo could weaken the turbulence. In particular, the
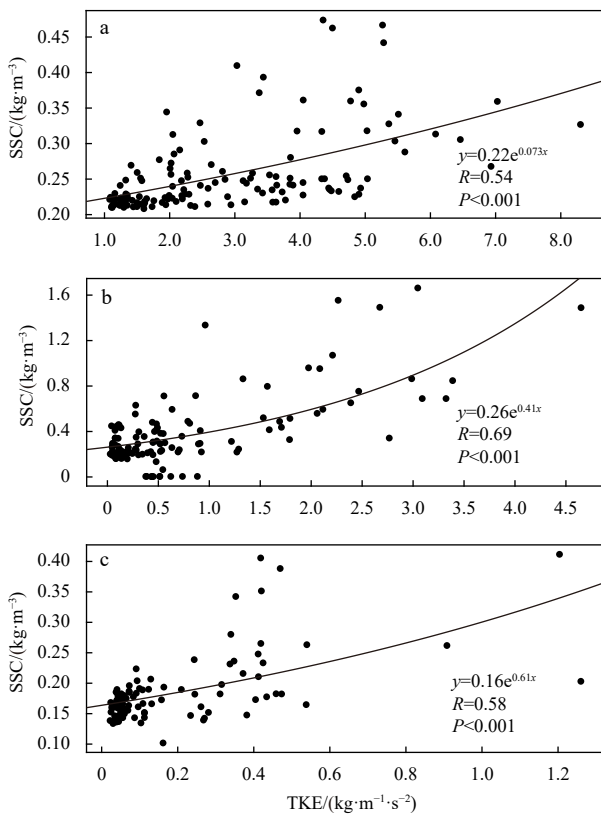
coastal arrangement and plum-shape layout of bamboo fences made the porosity as high as 95%, which ensured tidewater movement, so small animals could travel freely during the flood and ebb tide. The water that stayed in the strips gaps after the tide cycles provided habitats for animals to spawn and reproduce, which preserved the integrity of wetland ecosystem. The implementation of the bamboo fences experiment in a local area of Qixing Island of the Nanliu River, has promoted the bare flat siltation of the middle tidal flat by about 50%. Significant siltation was observed in the field, and ripples were formed in many places (Figs 6b, c and 11a, b). Around 3–4 cm of bamboo remained above the bed after 9 months, which was not enough for hydrodynamic weakening in November compared with that in March. At the same time, local scouring disappeared while depositions were observed on both sides of bamboo fences (Fig. 11b). Multiple small animal caves (Fig. 11a) and mangrove seedlings (Fig. 11c) were found between bamboo fences, indicating that bamboon fences induced hydrodynamic mitigation developed a safe environment for mangrove seeds and fruits. Currents can carry seeds between vegetation populations and successfully establish biological connections (Van der Stocken et al., 2019). The effective diffusion mechanism accelerated the mangrove forests expansion, and ultimately promoted the tidal flat silting to meet the social demands.

5 Conclusions

In recent years, under the background of SLR and in view of the limitations of grey seawalls, green structures have gradually attracted worldwide attention because of the sustainability in flood control and environment protection. A new ecological technology composed of bamboo fences was explored to conduct silting experiments on mangroves tidal flat in the Nanliu Delta, and to discuss the hydrodynamic deposition processes during spring tides. The main conclusions were as follows:
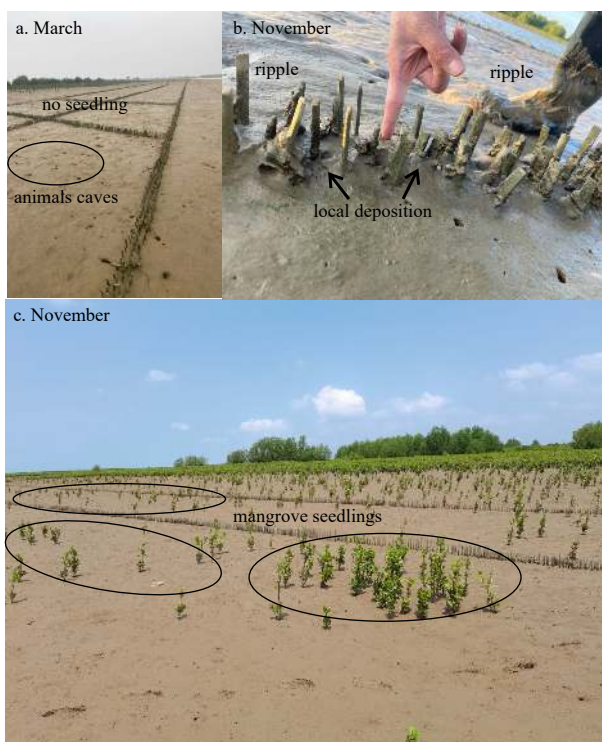

Fig. 11. View of bamboo fences contributed to animal habitat (a), sediment deposition (b), and mangrove expansion (c) so far.

(1) Under the same sediment substrate condition, bamboo fences, rather than the topographic slope, was the main factor slowing down the hydrodynamic. The flow direction was dispersed through the bamboo area during flood tide, and the mean horizontal flow velocity U_m decreased by more than 40%. Moreover, bamboo fences served as the edge of mangroves increasing the width of *A. corniculatum* forests during ebb tide.

(2) The turbulent kinetic energy dissipation rate ε increased greatly in bamboo area, reaching 2.48×10^{-5} m²·Hz/s², where bamboo fences weakened the sediment incipient motion and intercepted the suspended sediment. The reduction of suspended sediment flux in bamboo area resulted in the siltation rate of the bed surface being 140% and 29.3% higher than that of the bare flat and mangroves, respectively.

(3) Compared with the current silting promotion engineering, the bamboo fences project had the advantages of biodegradability, economy, lightness and ecological protection, which not only produced better siltation effect, but also provided habitats for tidal flat animals and ensured the growth environment of mangrove seedlings.

References

Analuddin K, Septiana A, Jamili, et al. 2020. Sea level rise impact on mangrove growth and development in Coral Triangle Ecoregion Southeast, Indonesia. IOP Conference Series: Materials Science and Engineering, 797(1): 012036, doi: 10.1088/1757-899X/797/1/012036

Atwood T B, Connolly R M, Almahasheer H, et al. 2017. Global patterns in mangrove soil carbon stocks and losses. Nature Climate Change, 7(7): 523–528, doi: 10.1038/nclimate3326

Brinkman R M. 2006. Wave attenuation in mangrove forests: an investigation through field and theoretical studies [dissertation]. Townsville, Queensland: James Cook University

Bulleri F, Chapman M G. 2010. The introduction of coastal infrastructure as a driver of change in marine environments. Journal of Applied Ecology, 47(1): 26–35, doi: 10.1111/j.1365-2664.2009.01751.x

Butt T, Russell P. 1999. Suspended sediment transport mechanisms in high-energy swash. Marine Geology, 161(2–4): 361–375

Chanson H, Trevethan M, Aoki S I. 2008. Acoustic Doppler velocimetry (ADV) in small estuary: Field experience and signal post-processing. Flow Measurement and Instrumentation, 19(5): 307–313, doi: 10.1016/j.flowmeasinst.2008.03.003

Christensen D F, Brinkkemper J, Ruessink G, et al. 2018. Field observations of turbulence in the intertidal and shallow subtidal zones. Continental Shelf Research, 170: 21–32, doi: 10.1016/j.csr.2018.10.002

Dai Zhijun, Zhou Xiaoyan, Wang Jie, et al. 2021. Review and prospect of mangrove tidal flat sedimentary dynamics. Journal of Tropical Oceanography (in Chinese), 40(3): 69–75

Dao H T, Hofland B, Stive M J F, et al. 2020. Experimental assessment of the flow resistance of coastal wooden fences. Water, 12(7): 1910, doi: 10.3390/w12071910

Dao T, Stive M J F, Hofland B, et al. 2018. Wave damping due to wooden fences along mangrove coasts. Journal of Coastal Research, 34(6): 1317–1327, doi: 10.2112/JCOASTRES-D-18-00015.1

FAO. 2020. Global forest resources assessment 2020: Main report. Rome: FAO

Foster-Martinez M R, Lacy J R, Ferner M C, et al. 2018. Wave attenuation across a tidal marsh in San Francisco Bay. Coastal Engineering, 136: 26–40, doi: 10.1016/j.coastaleng.2018.02.001

Foti E, Musumeci R E, Stagnitti M. 2020. Coastal defence techniques

and climate change: a review. Rendiconti Lincei. Scienze Fisiche e Naturali, 31(1): 123–138

Friedrichs C T. 2011. Tidal flat morphodynamics. In: Flemming B W, Hansom J D, eds. Treatise on Estuarine and Coastal Science. Volume 3: Estuarine and Coastal Geology and Geomorphology. London: Academic Press, 137–170

Furukawa K, Wolanski E, Mueller H. 1997. Currents and sediment transport in mangrove forests. Estuarine, Coastal and Shelf Science, 44(3): 301–310

Gong Zheng, Geng Liang, Lv Yuting, et al. 2017. Mechanisms underlying the dynamic evolution of an open-coast tidal flat-creek system: II: influence of tidal range. Advances in Water Science (in Chinese), 28(2): 231–239

Goring D G, Nikora V I. 2002. Despiking acoustic Doppler velocimeter data. Journal of Hydraulic Engineering, 128(1): 117–126, doi: 10.1061/(ASCE)0733-9429(2002)128:1(117)

Green M O. 1992. Spectral estimates of bed shear stress at subcritical Reynolds numbers in a tidal boundary layer. Journal of Physical Oceanography, 22(8): 903–917, doi: 10.1175/1520-0485 (1992)022<0903:SEOBSS>2.0.CO;2

Horstman E M, Dohmen-Janssen C M, Bouma T J, et al. 2015. Tidal-scale flow routing and sedimentation in mangrove forests: combining field data and numerical modelling. Geomorphology, 228: 244–262, doi: 10.1016/j.geomorph.2014.08.011

Horstman E M, Dohmen-Janssen C M, Narra P M F, et al. 2014. Wave attenuation in mangroves: A quantitative approach to field observations. Coastal Engineering, 94: 47–62, doi: 10.1016/j. coastaleng.2014.08.005

Hu Zhan, Lian Simei, Wei Huaiyu, et al. 2021. Laboratory data on wave propagation through vegetation with following and opposing currents. Earth System Science Data, 13(10): 4987–4999, doi: 10.5194/essd-13-4987-2021

Hu Zhan, Lian Simei, Zitman T, et al. 2022. Wave breaking induced by opposing currents in submerged vegetation canopies. Water Resources Research, 58(4): e2021WR031121, doi: 10.1029/2021 WR031121

Hu Zhan, Suzuki T, Zitman T, et al. 2014. Laboratory study on wave dissipation by vegetation in combined current–wave flow. Coastal Engineering, 88: 131–142, doi: 10.1016/j.coastaleng. 2014.02.009

Huntley D A. 1988. A modified inertial dissipation method for estimating seabed stresses at low Reynolds numbers, with application to wave/current boundary layer measurements. Journal of Physical Oceanography, 18(2): 339–346, doi: 10.1175/1520-0485(1988)018<0339:AMIDMF>2.0.CO;2

Li Yanhong, Chen Qinqin, Yu Guoliang. 2007. Advances and prospects in study on siltation promotion and erosion control techniques for beach sediments. Coastal Engineering (in Chinese), 26(4): 27–34

Liu Zhiyu, Wei Hao. 2007. Estimation to the turbulent kinetic energy dissipation rate and bottom shear stress in the tidal bottom boundary layer of the Yellow Sea. Progress in Natural Science, 17(3): 289–297, doi: 10.1080/10020070612331343260

Long Chuqi, Dai Zhijun, Wang Riming, et al. 2022. Dynamic changes in mangroves of the largest delta in northern Beibu Gulf, China: Reasons and causes. Forest Ecology and Management, 504: 119855, doi: 10.1016/j.foreco.2021.119855

Lovelock C E, Cahoon D R, Friess D A, et al. 2015. The vulnerability of Indo-Pacific mangrove forests to sea-level rise. Nature, 526(7574): 559–563, doi: 10.1038/nature15538

Mai Van C, Ngo A, Mai T, et al. 2021. Bamboo fences as a nature-based measure for coastal wetland protection in Vietnam. Frontiers in Marine Science, 8: 756597, doi: 10.3389/fmars.2021. 756597

Maza M, Adler K, Ramos D, et al. 2017. Velocity and drag evolution from the leading edge of a model mangrove forest. Journal of Geophysical Research: Oceans, 122(11): 9144–9159, doi: 10.1002/2017JC012945

Mazda Y, Magi M, Kogo M, et al. 1997. Mangroves as a coastal protection from waves in the Tong King delta, Vietnam. Mangroves & Salt Marshes, 1(2): 127–135

Möller I, Spencer T, French J R, et al. 1999. Wave transformation over salt marshes: a field and numerical modelling study from North Norfolk, England. Estuarine, Coastal & Shelf Science, 49(3): 411–426

Montgomery J M, Bryan K R, Mullarney J C, et al. 2019. Attenuation of storm surges by coastal mangroves. Geophysical Research Letters, 46(5): 2680–2689, doi: 10.1029/2018GL081636

Morris R L, Konlechner T M, Ghisalberti M, et al. 2018. From grey to green: Efficacy of eco-engineering solutions for nature-based coastal defence. Global Change Biology, 24(5): 1827–1842, doi: 10.1111/gcb.14063

Murray N J, Phinn S R, Dewitt M, et al. 2019. The global distribution and trajectory of tidal flats. Nature, 565(7738): 222–225, doi: 10.1038/s41586-018-0805-8

Murray N J, Worthington T A, Bunting P, et al. 2022. High-resolution mapping of losses and gains of Earth's tidal wetlands. Science, 376(6594): 744–749, doi: 10.1126/science.abm9583

Pang Wenhong, Dai Zhijun, Ma Binbin, et al. 2020. Linkage between turbulent kinetic energy, waves and suspended sediment concentrations in the nearshore zone. Marine Geology, 425: 106190, doi: 10.1016/j.margeo.2020.106190

Pang Wenhong, Zhou Xiaoyan, Dai Zhijun, et al. 2021. ADV-based investigation on bed level changes over a meso-macro tidal beach. Frontiers in Marine Science, 8: 733923, doi: 10.3389/ fmars.2021.733923

Parsheh M, Sotiropoulos F, Porté-Agel F. 2010. Estimation of power spectra of acoustic-Doppler velocimetry data contaminated with intermittent spikes. Journal of Hydraulic Engineering, 136(6): 368–378, doi: 10.1061/(ASCE)HY.1943-7900.0000202

Paul M, Bouma T J, Amos C L. 2012. Wave attenuation by submerged vegetation: combining the effect of organism traits and tidal current. Marine Ecology Progress Series, 444: 31–41, doi: 10. 3354/meps09489

Santa Barbara-University of California. 2017. Seawalls: Ecological effects of coastal armoring in soft sediment environments. ScienceDaily. https://www.sciencedaily.com/releases/2017/07/170724 133156.htm[2022-06-10]

Shepard F P. 1954. Nomenclature based on sand-silt-clay ratios. Journal of Sedimentary Research, 24(3): 151–158

Stapleton K R, Huntley D A. 1995. Seabed stress determinations using the inertial dissipation method and the turbulent kinetic energy method. Earth Surface Processes and Landforms, 20(9): 807–815, doi: 10.1002/esp.3290200906

Stefanon L, Carniello L, D'Alpaos A, et al. 2010. Experimental analysis of tidal network growth and development. Continental Shelf Research, 30(8): 950–962, doi: 10.1016/j.csr.2009.08.018

Taylor G I. 1938. The spectrum of turbulence. Proceedings of the Royal Society of London. Series A-Mathematical and Physical Sciences, 164(919): 476–490

Van Der Stocken T, Carroll D, Menemenlis D, et al. 2019. Global-scale dispersal and connectivity in mangroves. Proceedings of the National Academy of Sciences of the United States of America, 116(3): 915–922, doi: 10.1073/pnas.1812470116

van Santen P, Augustinus P G E F, Janssen-Stelder B M, et al. 2007. Sedimentation in an estuarine mangrove system. Journal of Asian Earth Sciences, 29(4): 566–575, doi: 10.1016/j.jseaes. 2006.05.011

Wentworth C K. 1922. A scale of grade and class terms for clastic sediments. The Journal of Geology, 30(5): 377–392, doi: 10.1086/ 622910

Wiberg P L, Sherwood C R. 2008. Calculating wave-generated bottom orbital velocities from surface-wave parameters. Computers & Geosciences, 34(10): 1243–1262

Woodroffe C D. 1995. Response of tide-dominated mangrove shorelines in Northern Australia to anticipated sea-level rise. Earth Surface Processes & Landforms, 20(1): 65–85

Zhou Xiaoyan, Dai Zhijun, Pang Wenhong, et al. 2022. Wave attenuation over mangroves in the Nanliu Delta, China. Frontiers in Marine Science, 9: 874818, doi: 10.3389/fmars.2022.874818

Zhu Qin, Van Prooijen B C, Wang Zhengbing, et al. 2017. Bed-level changes on intertidal wetland in response to waves and tides: A case study from the Yangtze River Delta. Marine Geology, 385: 160–172, doi: 10.1016/j.margeo.2017.01.003